Journal of Radiological Science and Technology, 42(1), 39-46 ISSN 2384-1168(On-line) ISSN 2288-3509(Print)

<원저>

ACR 팬텀을 이용한 Cartesian Trajectory와 MultiVane Trajectory의 비교분석 : 영상강도 균질성과 저대조도 검체 검출률 test를 사용하여

남순권[1)]·최준호[1,2)]

[1)]강원대학교 물리학과·[2)]강원대학교병원 영상의학과

Comparative Analysis of Cartesian Trajectory and MultiVane Trajectory Using ACR Phantom in MRI : Using Image Intensity Uniformity Test and Low-contrast Object Detectability Test

Nam Soon-Kwon[1)]·Choi Joon-Ho[1,2)]

[1)]*Department of Physics, Kangwon National University*

[2)]*Department of Radiology, Kangwon National University Hospital*

Abstract This study conducted a comparative analysis of differences between cartesian trajectory in a linear rectangular coordinate system and MultiVane trajectory in a nonlinear rectangular coordinate system axial T1 and axial T2 images using an American College of Radiology(ACR) phantom. The phantom was placed at the center of the head coil and the top-to-bottom and left-to-right levels were adjusted by using a level. The experiment was performed according to the Phantom Test Guidance provided by the ACR, and sagittal localizer images were obtained. As shown in Figure 2, slices # 1 and # 11 were scanned after placing them at the center of a 45° wedge shape, and a total of 11 slices were obtained. According to the evaluation results, the image intensity uniformity(IIU) was 93.34% for the cartesian trajectory, and 93.19% for the MultiVane trajectory, both of which fall under the normal range in the axial T1 image. The IIU for the cartesian trajectory was 0.15% higher than that for the MultiVane trajectory. In axial T2, the IIU was 96.44% for the cartesian trajectory, and 95.97% for the MultiVane trajectory, which fall under the normal range. The IIU for the cartesian trajectory was by 0.47% higher than that for the MultiVane trajectory. As a result, the cartesian technique was superior to the MultiVane technique in terms of the high-contrast spatial resolution, image intensity uniformity, and low-contrast object detectability.

Key Words : Cartesian, MultiVane, ACR phantom, Image intensity Uniformity

중심 단어 : 데카르트, 다중날개, 미국방사선의학회 팬텀, 영상강도균질성

Ⅰ. Introduction

High-resolution magnetic resonance imaging(MRI) is a typical method for examining the human body by using nonionizing radiation. High-resolution MRI is a method using a magnetic field and radio frequency(RF) that are harmless to the human body, which is characterized by excellent spatial resolution and contrast resolution[1, 2]. The space in which the MRI stores data is called k-space. Among the various methods to obtain the data by filling the data in the k-space, the cartesian method, which is a scanning

Corresponding author: Joon-Ho Choi, Department of Radiology, Kangwon National University Hospital, 156, Baengnyeong-ro, Chuncheon-si, Gangwon-do, 24289, Republic of Korea / E-mail: jhchoi928@nate.com
Received 03 February 2019; Revised 18 February 2019; Accepted 25 February 2019

method in the cartesian coordinate system, is to fill the data in the frequency encoding direction[3]. The advantage of cartesian sampling is that the contrast of the image can be easily adjusted through the effective time of echo(TE) of the array corresponding to the contrast of the k-space[4-7]. However, as each row is linearly acquired in proportion to the number of phase encoding arrays, the involuntary motions of patients lead to various artifacts in the phase encoding direction[8]. As a result, artifacts are generated linearly throughout the image, so that the target region to be viewed is covered with artifacts hindering accurate images from being obtained. The MultiVane scanning method in a nonrectangular coordinate system is a noncartesian technique that oversamples the center of the k-space using separate vanes[9-12]. Each vane includes a k-space sample corresponding to the same low-resolution image. The data are collected in a series of revolving vanes, and each revolving vane collects the data from the central region of the k-space[13, 14]. The MRI phantom and protocol of the American College of Radiology(ACR) were developed by the ACR in 1992, and this MRI phantom could be applied to all types of MRI equipment[15]. Quantitative tests such as geometric accuracy, high-contrast spatial resolution, image intensity uniformity, and low-contrast object detectability have been performed by using ACR phantom[16]. In actual clinical setting, the MultiVane scanning method is used for motion compensation. This study was performed a comparative analysis of differences between cartesian trajectory and MultiVane trajectory in axial T1 and axial T2 images by using the ACR phantom to provide the basic clinical data.

II. Material and Methods

1. Material and equipment

The equipment used in this study includes a 3.0 T MRI(Achieva, Philips, Netherlands) and the ACR phantom. The ACR phantom is an acrylic plastic with both ends closed, having a length of 148 mm and a diameter of 190 mm. The inside of the phantom is filled with a solution of 10 mM of nickel chloride ($NiCl_2$) and 75 mM of sodium chloride (NaCl). The ACR phantom can be divided into a large phantom and a small phantom. The large phantom is designed for use in a head coil, which is used for quality control of most MRI equipment. The small phantom is designed for use in a knee coil[17]. As shown in Figure 1, the surface of the large phantom is marked with NOSE and CHIN, which helps determine the location of the phantom in the head coil[16, 18].

As show in Table 1, the used parameters were the same as those used in the actual clinical setting

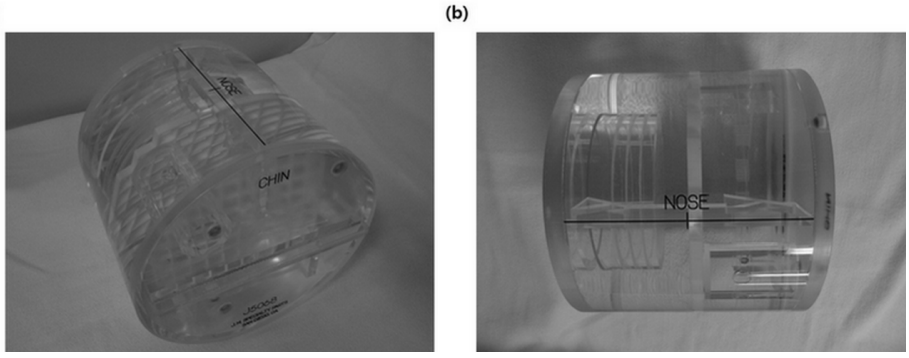

Fig. 1. Oblique (a) and lateral (b) views of a large ACR phantom

Table 1. Imaging parameters of the axial T1 and axial T2 sequence

Sequence	TR(ms)	TE(ms)	Matrix	FOV(mm)	Slice thickness(mm)	Gap(mm)	Number of slice
Axial T1	2,000	30	400×296	230	5	5	11
Axial T2	3,026	100	372×266	230	5	5	11

2. Measurement Methods

The phantom was placed at the center of the head coil and the top-to-bottom and left-to-right levels were adjusted by using a level. The experiment was performed according to the Phantom Test Guidance provided by the ACR, and sagittal localizer images were obtained. As shown in Figure 2, slices # 1 and # 11 were scanned after placing them at the center of a 45° wedge shape, and a total of 11 slices were obtained. Multivane trajectory and Cartesian trajectory were compared in actual brain axial T1 images.

The geometric accuracy is to evaluate whether the length in the image represents the actual length of the object. The lengths of slices # 1 and # 5 were measured in axial T1 and T2 in left-to-right, top-to-bottom, and both diagonal directions. The normal range was set as 190±2 mm for the inner diameter of the phantom. The high-contrast spatial resolution is to evaluate the ability to analyze small objects when the contrast-to-noise ratio(CNR) is sufficiently high. The resolution insert consists of an upper left(UL) and a lower right(LR) with diameters of 1.1 mm on the left, 1.0 mm in the middle, and 0.9 mm on the right. The normal range in this assessment is ≤ 1.0 mm. The arrangement of the resolution insert is composed of upper left(UL) and lower right(LR). The result values of image intensity uniformity are represented as the value calculated according to the percent integral uniformity(PIU) formula[16] as shown in Equation(1).

$$PIU = 100 \times [\,1 - \{\,(high - low)/(high + low)\,\}] \quad (1)$$

A region of interest (ROI) of 190-205 cm^2 was draw in slice #7. The window width and window level was adjusted to display the highest part and the lowest part of the signal intensity (mean pixel value) as an area of interest of 1 cm^2 in the whole area of interest. The value obtained by substituting the measured value at that part into the PIU formula corresponds to the IIU. The normal range is equal to or greater than 82%. Low-contrast object detectability is used to assess by what degree of contrast an object can be distinguished in an image. In the case of 3 T, the normal range for the low-contrast object detectability is 37 spokes.

3. Motion compensation in MultiVane

The motion compensation algorithm used in MultiVane consists of several imaging correction steps. First, the average blade(RB_0) of all the blades that were not corrected is calculated. Second, a single blade(RB_1) showing the best correlation with RB_0 is selected, a correlation with RB_1 is measured for each of the other blades, and the expected shift is applied to each blade. This average is formed after imparting the first weight to each blade according to the correlation with RB_1. Third, all the blades including RB_1 are relocated, and a new average blade(RB_2) is repeatedly generated. This process is iterated for the average blade RB_i until the last motion compensation is completed for the

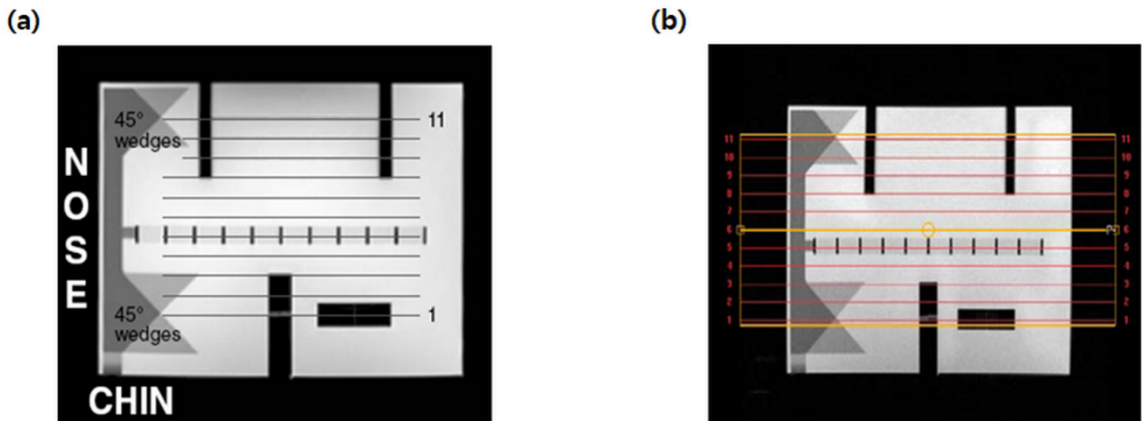

Fig. 2. Sagittal localizer showing the 11 required axial slice locations and paired 45° wedges. The words CHIN and NOSE on this image indicate the locations

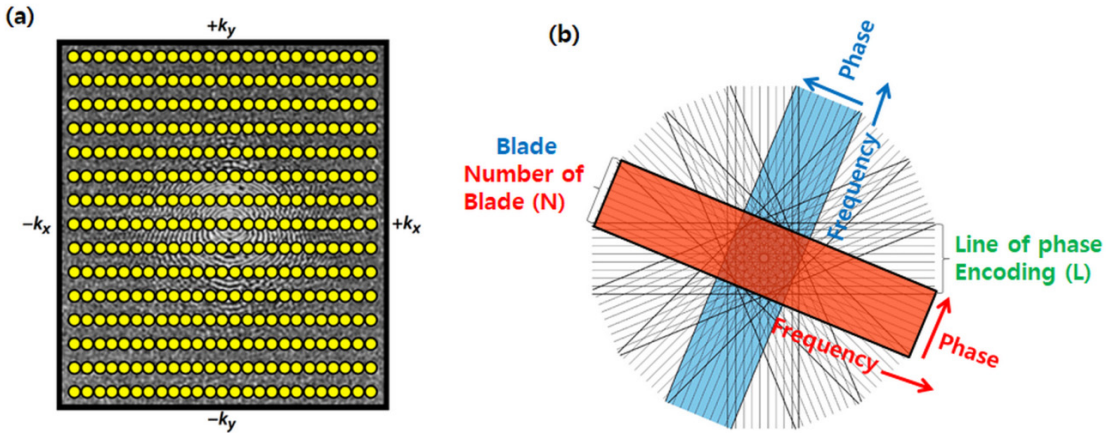

Fig. 3. The Cartesian sampling of k-space (a) and the graphic depiction of MultiVane k-space data acquisition (b) Data are acquired in a series of rotating vanes. Each vane contains several phase encoding lines

average blade RB_i+1. As shown in Figure 3, N blades and k-space with a diameter of L are resampled as the blade for every strip rotating with respect to the center of the k-space, and the data are acquired by superimposing with the strip. Assuming that the two blades are f_i and f_j and that the streaks from the X axis δ_i and δ_j the correlation between these two blades can be calculated based on Perceval's theorem, which is shown in the Equation (2).

$$\rho_{ij}(\delta_i-\delta_j)=\frac{\int f_i(x-\delta_i)f_j^*(x-\delta_j)dx}{\sqrt{\int|f_i(x)|^2dx\int|j(x)|^2dx}} \quad (2)$$

$$=\frac{\int F_i(k)F_j^*(k)e^{ik(\delta_i-\delta_j)dk}}{\sqrt{\int|F_i(k)|^2dk\int|F_j(k)|^2}}$$

where F_i and F_j are the results of the Fourier transforms for f_i and f_j respectively, and the relative motion of $(\delta_i-\delta_j)$ can be predicted by the maximum correlation between the two blades[20].

Ⅲ. Results

Table 2 shows the results of geometric accuracy. The length values for both cartesian and MultiVane trajectories are within the normal range of 190±2 mm. Table 3 shows the results of high-contrast spatial resolution. The values in the cartesian trajectory were measured as 0.9 mm in both axial T1 and T2. The results were within the normal range. On the other hand, the values in MultiVane were 1.0 mm in axial T1, 0.9 mm for UL. However that of MultiVane was 1.1 mm for RL in axial T2 which was deviated from the normal range.

Figure 4 shows the results for the IIU. The normal range is equal to or greater than 82%. In axial T1, the IIU in the cartesian trajectory is 93.34%, and the IIU in the MultiVane trajectory is 93.19%, which all fall under the normal range. However, the IIU in the cartesian trajectory is by 0.15% higher than that of the MultiVane trajectory. In axial T2, the IIU in the cartesian trajectory is 96.44% and the IIU in the MultiVane trajectory is 95.97%, which all fall under the normal range. However, the IIU in the cartesian trajectory is by 0.47% higher than that of the MultiVane trajectory.

Figure 5 shows low-contrast object detectability. In axial T1, the value in the cartesian trajectory was 38.4 spokes, which falls under the normal range, and the value in the MultiVane trajectory was 36.2 spokes, which deviated from the normal range. In axial T2, the value in the cartesian trajectory was 37.2 spokes cartesian, and the value in the MultiVane trajectory was 31.2 spokes. Thus, the value in the cartesian trajectory falls under the normal range, while the

Table 2. Results of the geometric accuracy test for k-space trajectory (cartesian and multivane)

Sampling method	Slice number	Item	Normal range	Measurement (mm)
Cartesian	Axial T1 #1	Top-to-Bottom	190±2 mm	190.40
		Left-to-Right		190.36
	Axial T1 #5	Top-to-Bottom	190±2 mm	189.64
		Left-to-Right		189.70
		Diagonal(Left-Right)		189.88
		Diagonal(Right-Left)		189.88
	Axial T2 #1	Top-to-Bottom	190±2 mm	188.96
		Left-to-Right		189.62
	Axial T2 #5	Top-to-Bottom	190±2 mm	189.56
		Left-to-Right		189.24
		Diagonal(Left-Right)		189.04
		Diagonal(Right-Left)		189.32
Multivane	Axial T1 #1	Top-to-Bottom	190±2 mm	190.06
		Left-to-Right		190.24
	Axial T1 #5	Top-to-Bottom	190±2 mm	190.18
		Left-to-Right		189.80
		Diagonal(Left-Right)		189.54
		Diagonal(Right-Left)		189.68
	Axial T2 #1	Top-to-Bottom	190±2 mm	189.74
		Left-to-Right		189.66
	Axial T2 #5	Top-to-Bottom	190±2 mm	188.92
		Left-to-Right		189.32
		Diagonal(Left-Right)		189.04
		Diagonal(Right-Left)		189.32

Table 3. Results of the high-contrast spatial resolution test for k-space trajectory (cartesian and multivane)

Sampling method	Slice number	Item	Normal range	Measurement(mm)
Cartesian	Axial T1 #1	UL	≤1.0 mm	0.9
		RL		0.9
	Axial T2 #1	UL	≤1.0 mm	0.9
		RL		0.9
Multivane	Axial T1 #1	UL	≤1.0 mm	1.0
		RL		1.0
	Axial T2 #1	UL	≤1.0 mm	0.9
		RL		1.1

value in the MultiVane trajectory was deviated from the normal range. Furthermore, the value in the MultiVane trajectory was deviated from the normal range by 2.16% in axial T1, and by 15.67% in the axial T2.

Figure 6 shows that cartesian images exhibit better contrast and sharpness than MultiVane images in actual brain MRI axial T1 images. Furthermore, the cartesian images are more clearly distinguished between gray matter and white matter

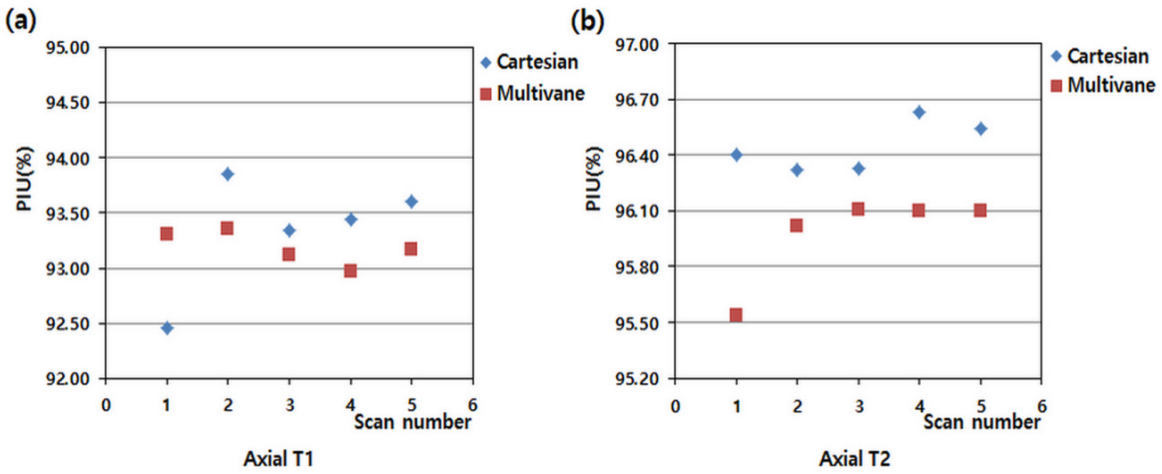

Fig. 4. PIU values in the image intensity uniformity test of cartesian and multivane for axial T1 (a) and axial T2 (b)

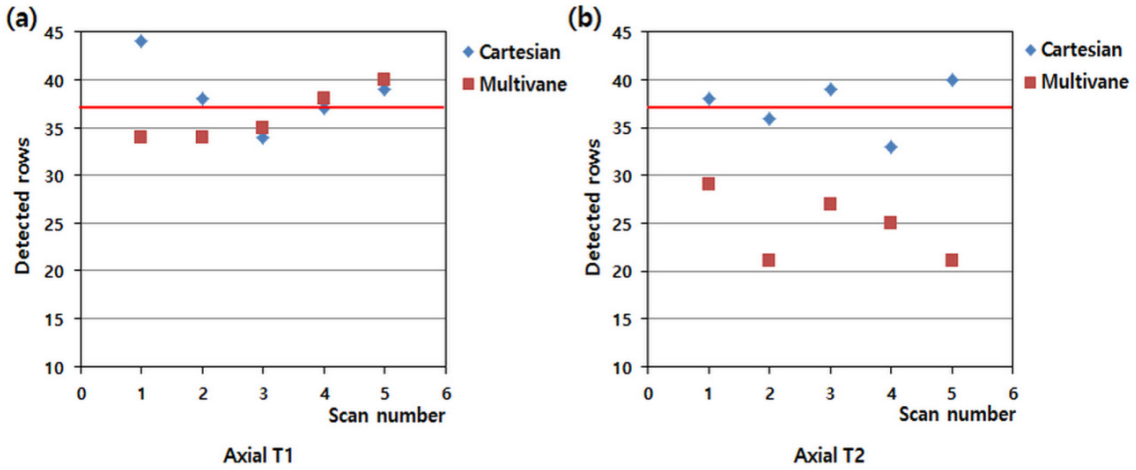

Fig. 5. Detected rows in the low-contrast object detectability test of cartesian and multivane for axial T1(a) and axial T2(b). The dashed lines(red line) indicate the ACR recommended acceptance value for 3.0 T (37 spokes)

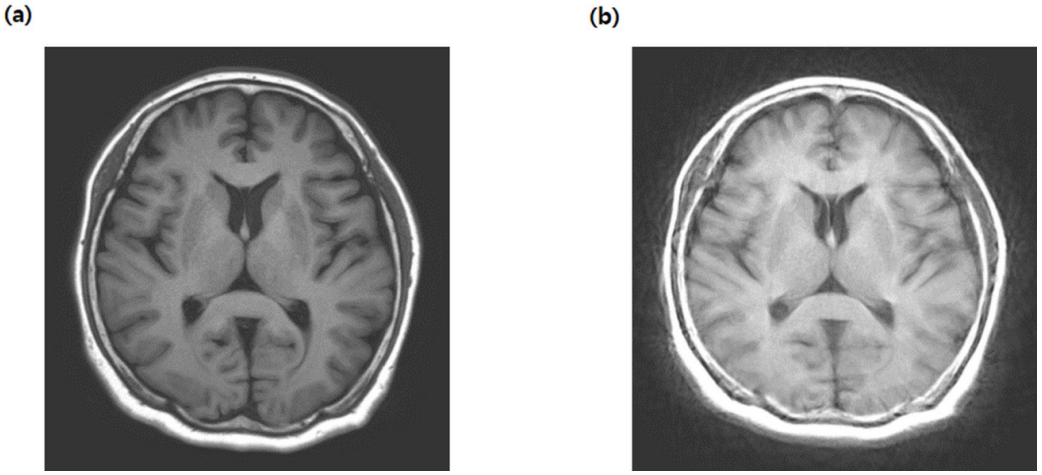

Fig. 6. Both images are axial T1 images for an image filled with k-space using Cartesian (a) and the image using the MultiVane trajectory (b). The shape of the blade can be seen in the image

Ⅳ. Discussion

Among the several techniques used to fill the k-space, the most commonly used technique is the cartesian trajectory. However, the cartesian technique generates various artifacts due to the involuntary motion of the patients in the phase encoding direction. In actual clinical setting, it is recommended to use the MultiVane technique instead of the cartesian technique to correct artifacts arising from the motion. Nevertheless, the MultiVane technique has not been commonly used because the time to create the images by filling the k-space becomes longer in the MultiVane technique. In this experiment, cartesian and multivane trajectories were compared and analyzed by using an ACR phantom in the absence of motion, although the MultiVane technique is for correcting artifacts arising from the motions in the cartesian trajectory. It would have been more helpful if we used a real phantom (Rando Phantom or anthropomorphic phantom) rather than an ACR phantom.

Ⅴ. Conclusions

According to the results, the geometric accuracy of both cartesian and MultiVane trajectories was within the normal range of 190±2 mm. The high-contrast spatial resolution in the cartesian trajectory was measured as 0.9 in both axial T1 and T2, which was within the normal range. The high-contrast spatial resolution in the MultiVane trajectory was measured as 1.0 in axial T1 and 0.9 for UL and 1.1 for RL in axial T2, in which RL was deviated from the normal range. The IIU was 0.15% higher in the cartesian trajectory than in the MultiVane trajectory in the axial T1. In axial T2, the cartesian trajectory showed 0.47% higher IIU than the MultiVane trajectory. The low-contrast object detectability was 38.4 spokes for the cartesian trajectory in axial T1, which falls under the normal range while low-contrast object detectability was 36.2 spokes for the MultiVane trajectory, which was deviated from the normal range. In axial T2, the value was 37.2 spokes for the cartesian trajectory, and 31.2 spokes for the MultiVane trajectory, in which the value in the cartesian trajectory falls under the normal range, while the value in the MultiVane trajectory was deviated from the normal range. As a result, the results of using the cartesian technique gave better results than the MultiVane technique in terms of the high-contrast spatial resolution, image intensity uniformity and low-contrast object detectability. This study would help obtain the basic data that can be used in actual clinical setting.

REFERENCES

[1] Zhu Z, Yang R, Zhang J, Zhang C. Compressed sensing MRI by Two-Dimensional wavelet filter banks. Int Workshop on Multidimensional (nD) Systems. 2011;1-6.

[2] Lee HB, Choi KW, Son SY. Usefulness analysis of radial non-cartesian trajectory in the high-resolution MRA. J Korea Academia-Industrial cooperation Soc. 2013;14(12):6284-9.

[3] Fujimoto K, Koyama T, Tamai K, Morisawa N, Okada T, Togashi K. BLADE acquisition method improves T2-weighted MR images of the female pelvis compared with a standard fast spin-echo sequence. Eur J Radiol. 2011;80:796-801.

[4] Levine E, Daniel B, Vasanawala S, Hargreaves B, Saranathan M. 3D Cartesian MRI with compressed sensing and variable view sharing using complementary poisson-disc sampling. Magn Reson Med. 2001;44(3):317-23.

[5] Zhu S, Gao S, Cheng L, Bao S. Review: K-Space trajectory development. International Conference on Mechanical Industrial and production engineering. 2013;356-60.

[6] d'Arcy J, Collins D, Rowland J, Padhani A, Leach M. Application of sliding window reconstruction with Cartesian sampling for dynamic contrast enhanced MRI. NMR Biomed. 2002;15:174-83.

[7] Saranathan M, Rettmann DW, Hargreaves BA, Clarke SE, Vasanawala SS. Differential subsampling with

cartesian ordering (DISCO): A high spatio-temporal resolution dixon imaging sequence for multiphasic contrast enhanced abdominal imaging. J Magn Reson Imaging. 2012;35(6):1484-92.

[8] Park SK, Ahn CB, Sim DG, Park HC. Study of motion effects in cartesian and spiral parallel MRI using computer simulation. J Korean Soc Magn Reson Med. 2008;12(2):123-30.

[9] Attenberger UI, Runge VM, Williams KD, et al. T1-Weighted brain imaging with a 32-channel coil at 3T using turboFLASH BLADE compared with standard cartesian k-space sampling. Invest Radiol. 2009;44(3):177-83.

[10] Wright KL, Hamilton JI, Griswold MA, Gulani V, Seiberlich N. Non-Cartesian parallel imaging reconstruction. J Magn Reson Imaging. 2014;40(5); 1022-40.

[11] Kang KA, Kim YK, Kim EJ, et al. T2-weighted liver MRI using the MultiVane technique at 3T: Comparison with conventional T2-weighted MRI. Korean J Radiol. 2015;16(5):1038-46.

[12] Ohshita T. Basic examination of an image charac-teristic in Multivane. Jpn J Radiological Technology. 2011;67(10):1298-303.

[13] Deng J, Larson AC. Multishot targeted PROPELLER magnetic resonance imaging: Description of the technique and initial applications. Invest Radiol. 2009;44(8):454-62.

[14] Haneder S, Dinter D, Gutfleisch A, Schoenberg SO, Michael HJ. Image quality of T2w-TSE of the abdo-men and pelvis with cartesian or BLADE type k-space sampling: A retrospective inter individual comparison study. Eur J Radiol. 2011;79:177-82.

[15] Reston, Phantom test guidance for the ACR MRI accreditation program. ACR; 1998.

[16] American College of Radiology: Phantom Test Gudiance for ACR MRI Accreditation Program, 2005.

[17] American Colleage of Radiology. Site Scanning Instructions for Use of MR Phantom for the ACRTM MRI Accreditation Program 2002 http://www.acr.org/~/media/ACR/Documents/Accreditation/MRI/Large Phantom Instruction. Pdf Accessed July 2. 2018.

[18] Kaljustea D, Nigulb M. Evaluation of the ACR MRI phantom for quality assurance tests of 1.5T MRI scanners in Estonian hospital. P Est Acad Sci. 2014;63(3):328-34.

[19] Lee JW, Ahn KJ, Lee SK, et al. Usefulness of ACR MRI phantom for quality assurance of MRI instruments. J Korean Radiol S. 2006;54:47-5.

[20] Lee SJ, Yu SM. The image evaluation of iterative motion correction reconstruction algorithm PROPELLER T2-weighted imaging compared with MultiVane T2-weighted imaging. J Korean Physical S. 2017;71(4):238-43.